

ChemComm

Accepted Manuscript



This is an *Accepted Manuscript*, which has been through the Royal Society of Chemistry peer review process and has been accepted for publication.

Accepted Manuscripts are published online shortly after acceptance, before technical editing, formatting and proof reading. Using this free service, authors can make their results available to the community, in citable form, before we publish the edited article. We will replace this *Accepted Manuscript* with the edited and formatted *Advance Article* as soon as it is available.

You can find more information about *Accepted Manuscripts* in the [Information for Authors](#).

Please note that technical editing may introduce minor changes to the text and/or graphics, which may alter content. The journal's standard [Terms & Conditions](#) and the [Ethical guidelines](#) still apply. In no event shall the Royal Society of Chemistry be held responsible for any errors or omissions in this *Accepted Manuscript* or any consequences arising from the use of any information it contains.



ChemComm

COMMUNICATION

Aqueous oxidation reaction enabled layer-by-layer corrosion of semiconductor nanoplates into single-crystalline 2D nanocrystals with single layer accuracy and ionic surface capping

Received 00th January 20xx,
Accepted 00th January 20xx

DOI: 10.1039/x0xx00000x

Muwei Ji^[a], Meng Xu^[a], Jun Zhang^[b], Jiajia Liu^[a], and Jiatao Zhang^{[a],*}

www.rsc.org/

Controllable aqueous oxidation reaction enabled layer-by-layer corrosion has been proposed to prepare high-quality two-dimensional (2D) semiconductor nanocrystals with single layer accuracy and well-kept hexagonal shapes. The appropriate oxidizing agent, such as H₂O₂, Fe(NO₃)₃, and HNO₃ could not only corrode the layered-crystalline-structured Bi₂Te₃ nanoplates layer-by-layer to be single quintuple layer, but also replace the organic barriers to be ionic ligands on the surface synergistically. The AFM analysis was used to confirm their layer-by-layer exfoliation from the side to the center. Together with precise XRD, LRTEM and HRTEM characterizations, the controllable oxidation reaction enabled aqueous layer-by-layer corrosion mechanism has been studied.

In order to get good prerequisite for enhanced functional performance, the synergistic taking away the organic insulating barriers and acquiring high-quality ultrathin single-crystalline nanosheets are expected.¹⁻³ Since the mechanical exfoliation using the scotch-tape method to prepare graphene from graphite and chemically oxidizing method with strong oxidants and ultrasonic cleavage to prepare graphene oxide from graphite,⁴⁻⁶ layered inorganic graphene analogues (IGA) with high percentage of surface atoms have recently inspired worldwide interests owing to their novel properties and great potential for applications in transistors,⁷⁻⁸ energy storage⁹⁻¹⁰ thermal conductors⁸ and topological insulators.¹¹⁻¹³ Many liquid methods, such as sonication in solvents,¹⁴ ion intercalation¹⁵⁻¹⁷ and surfactant-assisted exfoliation¹⁸ are used to prepare ultrathin nanosheets for applications where large quantities of materials are required, such as electrochemical energy storage,¹⁹⁻²⁰ catalysis,²¹⁻²² and sensing.²³⁻²⁵ The single-layer and multilayer nanosheets of layered IGA materials, such as transition metal chalcogenides,^{18, 19, 25, 26} metal oxides^{28, 29} and layered double hydroxides³⁰ have been prepared through

these methods. While the research progress on many kinds of such two-dimensional (2D) nanosheets, the 2D ultrathin nanocrystals with single-layer accuracy through facile liquid phase has only obtained limited progress. Especially, present liquid methods mostly still could not take away the concern of organic capping induced insulating barriers.³¹⁻³⁶ In order to get the efficient carriers transport in nanocrystals assembled film, the Talapin group reported that the inorganic ligands capped surface could facilitate the charge transport between nanocrystals.³⁷ P-group metals, because of their special electron properties, have potential applications in thermoelectricity,³⁸⁻³⁹ superconductivity,⁴⁰ magnetics⁴¹ and topological insulator.¹² Because of the oxidation-reduction potentials of Bi and Te elements, Bi₂Te₃ is easy to be oxidized when preparing in liquid phase, while it attracts lots of attention since its such applications.^{11, 42, 43} The 2D Bi₂Te₃ ultrathin nanosheets or films with single atomic layer accuracy and single-crystallinity mostly were obtained through molecule beam epitaxy (MBE) technology or chemical vapour deposition (CVD) by epitaxial growth.^{11, 12} The aqueous phase synthesis of high-quality 2D ultrathin Bi₂Te₃ nanocrystals with single atomic layer accuracy has been few reported, although there are many colloidal single-crystalline Bi₂Te₃ nanoplates reported.⁴⁴ As is known that, layered-crystalline-structured Bi₂Te₃ is oxidized in the air easily. The Yu group showed Te nanowires could be completely oxidized in the air and synthesized Te ultrathin nanowires from Te nanowire by oxidation.⁴⁵ Here, we take advantage of the oxidation reaction induced layer-by-layer corrosion to prepare single-layer level Bi₂Te₃ nanosheets controllably. With the appropriate choice of oxidizing agents, such as H₂O₂, Fe(NO₃)₃, and HNO₃, the nanoplates could be oxidized and corroded layer-by-layer. Most importantly, the synergistic ionic capping ligands could replace the original organic insulating barriers. Enabled by such, the 2D ultrathin Bi₂Te₃ nanocrystals with single layer accuracy have been successfully. Furthermore, this unprecedented mechanism of Bi₂Te₃ nanosheets formation has been proposed well.

a. Department: Beijing Key Laboratory of Construction Tailorable Advanced Functional Materials and Green Applications, School of Materials Science and Engineering, Beijing Institute of Technology, Beijing, 100081 (P. R. China)

b. Institute of semiconductors, Chinese Academy of Sciences, Beijing, 100083 (P.R.China)

E-mail: zhangjt@bit.edu.cn

Electronic Supplementary Information (ESI) available: [details of any supplementary information available should be included here]. See

COMMUNICATION

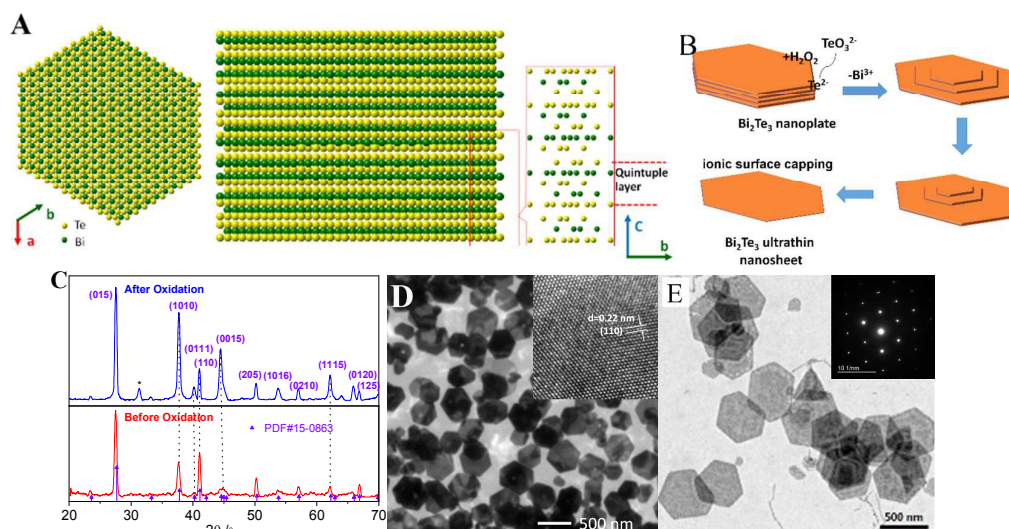


Figure 1. (A) Schematic of Bi_2Te_3 crystal structure: top view (left), front view and its quintuple layer (right); (B) Schematic of formation of Bi_2Te_3 nanosheets by oxidation reaction enabled exfoliation; (C) Powder XRD pattern comparison before and after oxidation, star (*) means the diffraction peak of Bi_2O_3 ; (D-E) TEM images of as-prepared Bi_2Te_3 nanoplates and nanosheets respectively; the inserts are the HRTEM image of nanoplate and the SAED pattern of one nanosheet. The inserts also showed the thickness of nanoplates and nanosheets by AFM analysis.

As the schematic crystal structure shown in Fig. 1A, single-crystalline Bi_2Te_3 consists of quintuple layers which connect each other by weak Van der Waals interactions.^{15, 31} Therefore, it is possible to exfoliate the layers in liquid phase by intercalating guest molecules and reducing the energy barrier.²⁷ Herein, we choose appropriate oxidization agents, such as H_2O_2 , $\text{Fe}(\text{NO}_3)_3$, and HNO_3 . Then Te^{2-} is oxidized into TeO_4^{2-} ($\text{Te}^{2-} + \text{H}_2\text{O}_2 \rightarrow \text{TeO}_4^{2-} + \text{H}_2\text{O}$). Simultaneously, the Bi^{3+} ions form into Bi_2O_3 ($2 \text{Bi}^{3+} + 6\text{OH}^- \rightarrow \text{Bi}_2\text{O}_3 + 3\text{H}_2\text{O}$) and take off from Bi_2Te_3 nanoplates because of the large lattice mismatch.⁴⁴ Especially, with the precise control of reaction kinetics, H_2O_2 could oxidize the crystal layers in Bi_2Te_3 nanoplates layer by layer from side into center. Finally, the quintuple-layered ultrathin 2D nanosheets formed, as the schematic growth mechanism shown in Fig. 1B. The XRD pattern of samples (Fig. 1C) showed that before and after oxidation, both nanoplates and nanosheets of Bi_2Te_3 display a pure rhombohedral phased Bi_2Te_3 and are in agreement with the standard XRD pattern (JCPDS # 15-0863). The difference of XRD pattern between before and after oxidation is the relative intensities of diffraction peaks because the oriented growth of ultrathin Bi_2Te_3 nanosheets becomes more and more obvious. As shown in Fig. 1C, after oxidation, the intensities of diffraction peaks, (1010), (0111), (0015) and (1115) peaks, become stronger while that of facets (110) become weaker (See the details in Table S1). It indicates that oxidation rate of various facets is different and the facets along a and b axis are corroded with higher reaction rates. However, the crystal phase remains the same during the corrosion process. The very small peaks of Bi_2O_3 coexist after oxidation because the trace Bi_2O_3 impurities in the sample, as shown in Figure S1. Due to the large lattice mismatch, Bi_2O_3 breaks away from Bi_2Te_3 nanosheets into small nanoparticles and can be removed by purification. TEM images of 2D Bi_2Te_3 nanocrystals in Fig. 1D-1E showed the

well-kept hexagonal morphologies before and after oxidation. The indexed lattice spacing of Bi_2Te_3 nanoplates and nanosheets kept as 0.22 nm, which is in agreement with the facets of (110) (also shown in Fig. S2). Furthermore, selective area electron diffraction (SAED) pattern of whole of one nanosheet are single-crystalline (Fig. 1E and Fig. S3).

In order to further clarify this special layer-by-layer oxidation corrosion, the controlled kinetics of oxidation reactions help us to get the intermediate state of Bi_2Te_3 nanoplates, as shown in Fig. 2A-2B and Fig. S2. There are a lot of stair-like Bi_2Te_3 nanoplates with thinner sides compared to the center part. Fig. 2A showed the morphologies of Bi_2Te_3 nanoplates during oxidation kept well and the edges of Bi_2Te_3 nanoplates are corroded firstly. The HRTEM image in Fig. 2B confirmed that the Bi_2Te_3 nanoplates maintained unchanged latticeorientations during the oxidation. The lattice spacings of two parts after different oxidation exfoliation are constant (0.22 nm), in agreement to facet (110). According to the mechanism of Bi_2Te_3 growth reported by Xiong and Jeong,⁴⁶⁻⁴⁷ Bi_2Te_3 nanoplate was growing with Te seed and new Bi_2Te_3 nanoparticles would attach the edge of seed and recrystallized. In comparison, the oxidation here occurred firstly on the surface, especially on the edge of top layers because of its higher Te^{2-} ions concentration. In such way, Bi_2Te_3 nanoplate is corroded layer by layer and the different oxidation rate results in the stair-like morphologies. Element mapping of Bi_2Te_3 nanoplates before and after oxidation (Fig. 2C-2D) also kept the same morphology and Bi_2Te_3 formation. Fig. 2 further verified this unprecedented oxidation process could corrode the nanoplates with layer-crystal structures into ultrathin nanosheets without shape and crystallization changing. The thickness changing before and after exfoliation was confirmed by AFM analysis. As shown in Fig S4, the as-prepared nanoplates were $\sim 50\text{nm}$ thick. The nanosheets finally could reach to $\sim 1.2\text{nm}$ thick (Fig. 3), which is equal to the thickness of quintuple layer.^{13, 28}

COMMUNICATION

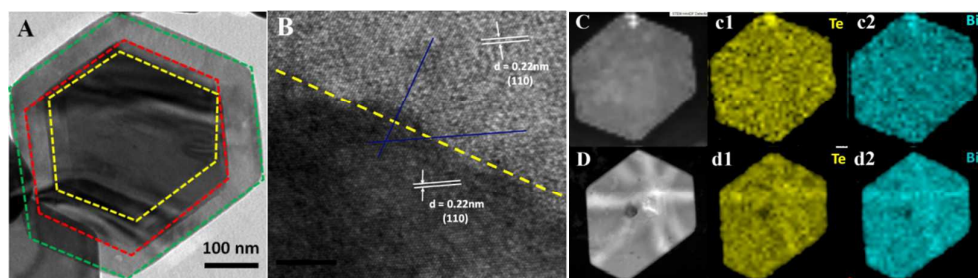


Figure 2. (A-B) HRTEM images of stair-like intermediate states during oxidation. The dotted lines were used to highlight the oxidation from outside to inside; (C-D) Element mapping of Bi_2Te_3 nanoplates before (C) and after (D) oxidation.

As shown in Fig. 3, AFM analysis was carried out to measure the height and surface morphologies of Bi_2Te_3 nanoplates at different steps of oxidation. As shown in Fig. 3A and Fig. S3-S4, the thickness of as-prepared Bi_2Te_3 nanoplates is about 50 nm. Then from Fig. 3B to Fig. 3C, the edges of Bi_2Te_3 nanoplate is firstly corroded by oxidation and then to be stair-like shape evidently. As shown in Fig. 2A and 3C, the thickness of Bi_2Te_3 edges became thinner while its lattice fringe remained. It meant that oxidation corroded Bi_2Te_3 nanoplate layers by layers. With the progress of oxidizing, the nanoplates become thinner and thinner. Finally, the nanoplate is corroded into 2D ultrathin nanosheets with 1.2 nm thickness, the single layer level (Fig. 3D).^{15, 31}

The XRD patterns evolutions of the powder samples under different concentrations of H_2O_2 , $\text{Fe}(\text{NO}_3)_3$ and HNO_3 were demonstrated to further confirm this special mechanism. From such, the sample's uniformity was also determined. As show in Fig. 4A, with more and more addition of H_2O_2 , the relative diffraction intensities of facet (006) and (0015) of Bi_2Te_3 nanosheets become stronger and that of facets (110) become weaker, while such of peak(015) has no obvious changing. Similar tendencies are also observed by using other oxidizing reagents, such as HNO_3 or $\text{Fe}(\text{NO}_3)_3$ (Fig. 4B). That means when the Bi_2Te_3 nanoplates are corroded into thin nanosheets, facets (006) and facets (0015) become more obvious.

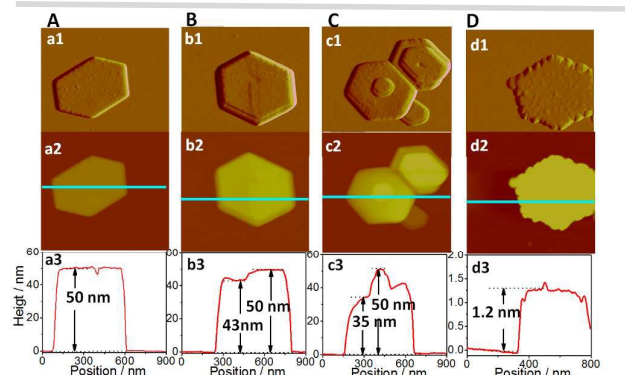


Figure 3. AFM images of Bi_2Te_3 nanoplates before (A) and during (B-D) the oxidation. a1, a2, a3, and a4 are their amplitude images; a2, b2, c2, d2 together with a3, b3, c3, d3 are their corresponding cross-sectional profiles along the blue line, respectively. The scan area: (A-C) $900\text{ nm} \times 900\text{ nm}$, (D) $800\text{ nm} \times 800\text{ nm}$.

Facet (110) is more active than other facets during oxidation. Hence, the relative XRD peak intensity of facet (110) became weaker. These phenomena confirms the exfoliation is along a and b axis. The changing of relative XRD peak intensities during oxidation confirmed the aggravated anisotropy of Bi_2Te_3 nanosheets and the effectiveness of this exfoliation strategy. Some oxidizing agents are used to react with Te^{2-} ions, single-crystalline Bi_2Te_3 nanoplates can be transformed into ultrathin single-crystalline nanosheets without morphology changing. As Xiong *et al.* reported, Raman characterization was sensitive to detect oxide phase existing in Bi_2Te_3 nanoplates.⁴⁸ In order to confirm no oxide phase existing on Bi_2Te_3 nanoplates, Raman characterization was employed. Firstly, the Raman spectra of five different individual Bi_2Te_3 nanoplates were collected, as shown in Fig. 4C and Figure S6. Secondly, the Raman spectra of as-prepared powder samples were also collected, as shown in Fig. S7. From these Raman spectra characterizations (see also S-1), No bismuth oxide phase was found on Bi_2Te_3 nanoplates. In other words, as-prepared ultrathin Bi_2Te_3 nanocrystals had high purity.

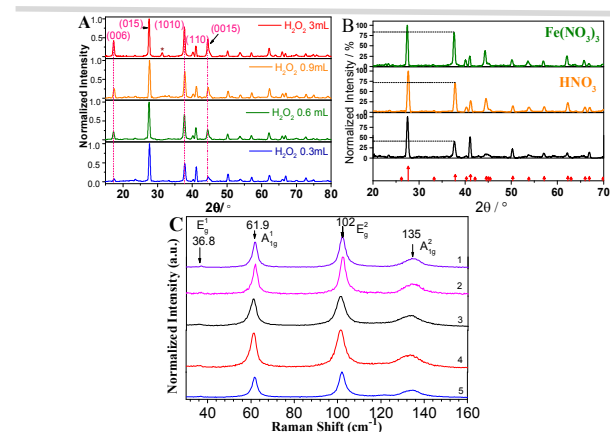


Figure 4. A) XRD patterns evolution of Bi_2Te_3 nanosheets oxidized by different concentrations of H_2O_2 ; B) XRD patterns comparison of Bi_2Te_3 nanosheets before (black line) and after oxidation by HNO_3 (orange line) and $\text{Fe}(\text{NO}_3)_3$ (Green line); C) Raman Spectra comparison of different individual Bi_2Te_3 nanoplates after oxidation.

In summary, a flexible aqueous oxidation enabled layer-by-layer corrosion process to prepare ultrathin 2D nanosheets has been established. Ultrathin 2D Bi_2Te_3 nanocrystals with single

layer accuracy have been unprecedentedly synthesized by this facile aqueous corrosion strategy with synergistic ionic ligands replacing process. By flexible choosing of oxidizing agents, Bi₂Te₃ nanoplates can be precisely corroded into single-crystalline ultrathin nanosheets with well-defined shape and layers control. It is also important that our approach should offer a general and constructive method to create wide range of ultrathin 2D semiconductor NCs with desired functionality, especially efficient charge transfer based on single-crystallization and ionic capping surface.

Acknowledgements

This work was supported by the Natural Science Foundation of China (21322105, 91323301, 51372025, 11574305, 51527901, 11225421, and 11434010), the Open Research Fund Program of the State Key Laboratory of Low-Dimensional Quantum Physics. We thank Prof. Chen Wang of National Center for Nanoscience and Technology, China for AFM measurements and helpful discussions.

Notes and references

- B. Radisavljevic; A. Radenovic; J. Brivio; V. Giacometti; A. Kis. *Nat. Nanotechnol.* 2011, **6**, 147.
- Q. Wang, K. Kalantar-Zadeh, A. Kis, J. N. Coleman, M. S. Strano, *Nat. Nanotechnol.* 2012, **7**, 699.
- Y. Zhu, S. Murali, M. D. Stoller, K. J. Ganesh, W. Cai, P. J. Ferreira, A. Pirkle, R. M. Wallace, K. A. Cychosz, M. Thommes, D. Su, E. A. Stach, R. S. Ruoff, *Science* 2011, **332**, 1537.
- K. S. Novoselov, A. K. Geim, S. V. Morozov, D. Jiang, Y. Zhang, S. V. Dubonos, I. V. Grigorieva, A. A. Firsov, *Science* 2004, **306**, 666.
- A. H. Castro Neto, F. Guinea, N. M. R. Peres, K. S. Novoselov, A. K. Geim, *Reviews of Modern Physics* 2009, **81**, 109.
- Hummers, W. S.; Offeman, R. E. *J. Am. Chem. Soc.* 1958, **80**, 1339.
- H. Li; J. Wu; Z. Yin; H. Zhang. *Acc. Chem. Res.* **2014**, **47**, 1067.
- H. Li; G. Lu; Y. Wang; Z. Yin; C. Cong; Q. He; L. Wang; F. Ding; T. Yu; H. Zhang. *Small* **2013**, **9**, 1974.
- Huang, X.; Tan, C.; Yin, Z.; Zhang, H. *Adv Mater* **2014**, **26**, (14), 2185.
- Tan, C.; Zhang, H. *Chem. Soc. Rev.* **2015**, **44**, (9), 2713.
- H. Peng, W. Dang, J. Cao, Y. Chen, D. Wu, W. Zheng, H. Li, Z. Shen, Z. Liu, *Nat. Chem.* 2012, **4**, 281.
- J. Zhang, C. Chang, P. Tang, Z. Zhang, X. Feng, K. Li, L. Wang, X. Chen, C. Liu, W. Duan, K. He, Q. Xue, X. Ma, Y. Wang, *Science* 2013, **339**, 1582.
- M. Lang, L. He, X. Kou, P. Upadhyaya, Y. Fan, H. Chu, Y. Jiang, J. H. Bardarson, W. Jiang, E. S. Choi, Y. Wang, N. Yeh, J. Moore, K. Wang, *Nano Lett.* 2013, **13**, 48.
- Y. Sun, Z. Sun, S. Gao, H. Cheng, Q. Liu, J. Piao, T. Yao, C. Wu, S. Hu, S. Wei, Y. Xie, *Nat. Commun.* 2012, **3**, 1057.
- T. Ludwig, L. Guo, P. McCrory, Z. Zhang, H. Gordon, H. Quan, M. Stanton, R. M. Frazier, R. D. Rogers, H. Wang, C. H. Turner, *Langmuir* 2015, **31**, 3644.
- Z. Zeng, T. Sun, J. Zhu, X. Huang, Z. Yin, G. Lu, Z. Fan, Q. Yan, H. H. Hng, H. Zhang, *Angew. Chem. Int. Ed.* 2012, **51**, 9052.
- Z. Zeng, Z. Yin, X. Huang, H. Li, Q. He, G. Lu, F. Boey, H. Zhang, *Angew. Chem. Int. Ed.* 2011, **50**, 11093.
- J. Han, S. Lee, J. Cheon, *Chem. Soc. Rev.* 2013, **42**, 2581.
- K. Xu, P. Chen, X. Li, Y. Tong, H. Ding, X. Wu, W. Chu, Z. Peng, C. Wu, Y. Xie, *J. Am. Chem. Soc.* 2015, **137**, 4119.
- X. Xia, J. Tu, Y. Zhang, J. Chen, X. Wang, C. Gu, C. Guan, J. Luo, H. Fan, *Chem. Mater.* 2012, **24**, 3793.
- Chen, J.; Wu, X. J.; Yin, L.; Li, B.; Hong, X.; Fan, Z.; Chen, B.; Xue, C.; Zhang, H. *Angew. Chem. Int. Ed.* **2015**, **54**, 1210.
- Zhou, W.; Yin, Z.; Du, Y.; Huang, X.; Zeng, Z.; Fan, Z.; Liu, H.; Wang, J.; Zhang, H. *Small* **2013**, **9**, 140.
- Tan, C.; Yu, P.; Hu, Y.; Chen, J.; Huang, Y.; Cai, Y.; Luo, Z.; Li, B.; Lu, Q.; Wang, L.; Liu, Z.; Zhang, H. *J. Am. Chem. Soc.* **2015**, **137**, (32), 10430.
- Zhang, Y.; Zheng, B.; Zhu, C.; Zhang, X.; Tan, C.; Li, H.; Chen, B.; Yang, J.; Chen, J.; Huang, Y.; Wang, L.; Zhang, H. *Adv Mater.* **2015**, **27**, (5), 935.
- S. Hu, X. Wang, *Chem. Soc. Rev.* 2013, **42**, 5577.
- M. Chhowalla, H. S. Shin, G. Eda, L. Li, K. P. Loh, H. Zhang, *Nat. Chem.* 2013, **5**, (4), 263.
- J. S. Son, J. H. Yu, S. G. Kwon, J. Lee, J. Joo, T. Hyeon, *Adv. Mater.* 2011, **23**, 3214.
- G. Shen, J. Xu, X. Wang, H. Huang, D. Chen, *Adv. Mater.* 2011, **23**, 771.
- E. Fortunato, P. Barquinha, R. Martins, *Adv. Mater.* 2012, **24**, 2945.
- V. Nicolosi, M. Chhowalla, M. G. Kanatzidis, M. S. Strano, J. N. Coleman, *Science* 2013, **340**, 1226419.
- Y. Zhao, R. W. Hughes, Z. Su, W. Zhou, D. H. Gregory, *Angew. Chem. Int. Ed.* 2011, **50**, 10397.
- T. Higashino, Y. Fujimori, K. Sugiura, Y. Tsuji, S. Ito, H. Imahori, *Angew. Chem. Int. Ed.* 2015, **54**, 9052.
- A. Chatterjee, K. Biswas, *Angew. Chem. Int. Ed.* 2015, **54**, 5623.
- H. Zhang, *ACS Nano* 2015, **9**, 9451.
- Y. Du, Z. Yin, J. Zhu, X. Huang, X. Wu, Z. Zeng, Q. Yan, H. Zhang, *Nat. Commun.* 2012, **3**, 1177.
- J. Feng, X. Sun, C. Wu, L. Peng, C. Lin, S. Hu, J. Yang, Y. Xie, *J. Am. Chem. Soc.* 2011, **133**, 17832.
- A. Nag, M. V. Kovalenko, J. Lee, W. Liu, B. Spokoyny, D. V. Talapin, *J. Am. Chem. Soc.* 2011, **133**, 10612.
- M. Scheele, N. Oeschler, K. Meier, A. Kornowski, C. Klinke, H. Weller, *Adv. Funct. Mater.* 2009, **19**, 3476.
- W. Shi, L. Zhou, S. Song, J. Yang, H. Zhang, *Adv. Mater.* 2008, **20**, 1892.
- M. Wang, C. Liu, J. Xu, F. Yang, L. Miao, M. Yao, C. Gao, C. Shen, X. Ma, X. Chen, Z. Xu, Y. Liu, S. Zhang, D. Qian, J. Jia, Q. Xue *Science* 2012, **336**, 52.
- L. Cheng, Z. Chen, S. Ma, Z. Zhang, Y. Wang, H. Xu, L. Yang, G. Han, K. Jack, G. Lu, J. Zou, *J. Am. Chem. Soc.* 2012, **134**, 18920.
- A. Soni, Y. Zhao, Y. Ligen, M. K. K. Aik, M. S. Dresselhaus, Q. Xiong, *Nano Lett.* 2012, **12**, 1203.
- G. Zhang, B. Kirk, L. A. Jauregui, H. Yang, X. Xu, Y. Chen, Y. Wu, *Nano Lett.* 2011, **12**, 56.
- H. Li, J. Cao, W. Zheng, Y. Chen, D. Wu, W. Dang, K. Wang, H. Peng, Z. Liu, *J. Am. Chem. Soc.* 2012, **134**, 6132.
- L. Xu, H. Liang, H. Li; K. Wang, Y. Yang, L. Song, X. Wang, S. Yu, *Nano Res.* 2015, **8**, 1081.
- Zhao, Y.; de la Mata, M.; Qiu, R. L. J.; Zhang, J.; Wen, X.; Magen, C.; Gao, X. P. A.; Arbiol, J.; Xiong, Q. *Nano Res.* **2014**, **7**, (9), 1243-1253.
- Min, Y.; Moon, G. D.; Kim, B. S.; Lim, B.; Kim, J.-S.; Kang, C. Y.; Jeong, U. *J. Am. Chem. Soc.* **2012**, **134**, (6), 2872-2875.
- Zhang, J.; Peng, Z.; Soni, A.; Zhao, Y.; Xiong, Y.; Peng, B.; Wang, J.; Dresselhaus, M. S.; Xiong, Q. *Nano Lett* **2011**, **11**, (6), 2407.